TECHNICAL RESEARCH REPORT

S Y S T E M S
R E S E A R C H
C E N T E R

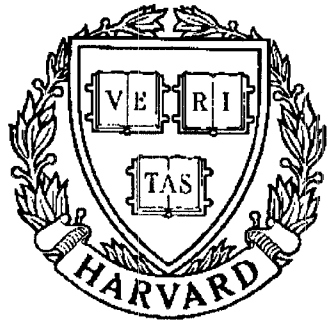

Supported by the National Science Foundation Engineering Research Center Program (NSFD CD 8803012), Industry and the University

Nonlinear Dynamics of Axial-Flow Compressors: A Parametric Study

by R.A. Adomaitis, D-C. Liaw, and E.H. Abed

TR 92-73

Nonlinear Dynamics of Axial-Flow Compressors: A Parametric Study

Raymond A. Adomaitis*, Der-Cherng Liaw†, and Eyad H. Abed‡

*Systems Research Center
University of Maryland
College Park, MD 20742

†Department of Control Engineering
National Chiao Tung University
Hsinhcu, 300, Taiwan, R.O.C.

‡Department of Electrical Engineering and
Systems Research Center
University of Maryland
College Park, MD 20742

Abstract

Analysis of the post-instability dynamical behavior of an axial-flow compression system model is carried out in a bifurcation-theoretic setting. Using global analysis techniques, we uncover the sequence of bifurcations in parameter space which allows us to rigorously determine whether the compressor stalls or surges when the throttle is slowly closed beyond the instability margin. Using these computational techniques, we also determine the conditions under which stalled and/or surging flow solutions *coexist* with the desired uniform-flow operating point and quantify the perturbations which destabilize this operating point.

Introduction

An important problem limiting the pressure rise of axial-flow gas compressors is the loss of stability of the steady, uniform flow field when the compressor is throttled down from the design operating point. Not only is it difficult to determine the operating conditions and system parameter values where the flow becomes unstable, but it is also not always clear what to expect as the post-instability, long term behavior—specifically, whether the compressor stalls or surges. Much attention has been devoted developing mathematical models which capture the different dynamical phenomena observed in compression systems. Numerical simulations with the models give insight into the operating conditions and which compression system parameters are important in governing the post-instability behavior. Analysis of how the dynamical behavior changes as parameters are varied can be used to predict the location of the instability margin.

One of the first nonlinear models that captured many of the observed compressor dynamical phenomena was developed by Greitzer [1]. The low-order model was derived from mass and momentum balances of the gas flow field averaged over the spatial domain. This approach lends itself very naturally to studying surge, since surge is a low frequency oscillation of the mean gas flow rate. However, the spatial details of the fluid flow rate variations along the compressor rotor cannot be resolved with this type of model, and so the rotating stall equilibrium appears as a steady state of much reduced pressure rise in this formulation. This means the compressor characteristic consists of three connected segments: two are the experimentally determined stable, uniform-flow and stalled-flow segments, connected by a segment of unstable stalled-flow equilibria that cannot be determined by experiments. Simulations were performed and compared to experimental results, and an important system parameter was identified as the factor determining the post-instability behavior. This parameter B consists of the ratio of the plenum volume to compressor volume for constant rotor speed. It was found that the compressor always stalls when throttled down for small values of B, and always surges for large values of B.

When studying a nonlinear model, a far more thorough analysis is possible with numerical bifurcation analysis compared to observations made with simple simulation. With these tools, we can compute and continue equilibrium solutions with respect to parameters, determine their stability, and find the bifurcations which mark qualitative changes in dynamical behavior. This type of analysis provides a framework in which to organize the dynamics exhibited by a particular system as the parameters vary. Thus, it is the ideal method for making sense of the diverse dynamics displayed by gas compression systems, for giving rigorous definitions to the instability margin, and for predicting the post-instability behavior.

The utility of the bifurcation analysis approach was first realized by McCaughan [2]. In that work, the numerical bifurcation analysis package AUTO [3] was used to study the more detailed compression system model of Moore and Greitzer [4]. This program can compute steady and periodic equilibrium solutions, compute certain bifurcations of equilibria, and can continue solutions and bifurcation points with respect to model parameters. However, some transitions in dynamical behavior cannot be computed with this package. These are bifurcations of the invariant structures of phase space (e.g., involving the stable and unstable manifolds of saddle points) and understanding these *global* bifurcations is required to determine the ranges of B where the different post-instability behaviors are found. Even in the simpler compressor model of Greitzer [1], global bifurcation analysis is required to uncover the sequence of bifurcations

that take place along the instability margin and determine whether the compressor surges or stalls. While we limit our analysis to the Greitzer model [1] and so cannot study important spatially-varying flow phenomena such as multiple stall cells [5,6] or the interplay of uniform-flow and nonuniform flow surge cycles [2], it will give us some insight into the global bifurcation phenomena to be expected as we continue this work with the more sophisticated models.

In addition to predicting the compression system dynamics after the uniform-flow operating point becomes *locally* unstable, another important benefit of global bifurcation analysis is that it reveals the parameter ranges where the locally stable uniform-flow operating point coexists with other stable equilibria (stable surge cycles and rotating stall equilibria). This allows us to determine the parameter regions where sufficiently large perturbations of the states drive the system from the uniform-flow operating point to another attractor. The destabilizing perturbations can also be precisely quantified in these regions of multistability by computing the boundary of the basin of attraction of the stable uniform-flow operating point. This basin boundary is found to consist of the saddle-stable manifold or an unstable limit cycle in the low-order model studied, the particular basin boundary structure depending on the compression system parameters.

The Model

A fourth-order, lumped-parameter model of an axial-flow gas compression system was developed in [1]. It is based on momentum balances of the mean gas flow through the compressor and throttle ducts, a gas mass balance over the plenum, and a linear correlation defining the time lag of the compressor pressure rise:

$$\begin{aligned}
\frac{dm_c}{dt} &= B(C - \Delta_p), \\
\frac{dm_t}{dt} &= \frac{B}{G}(\Delta_p - F), \\
\frac{d\Delta_p}{dt} &= \frac{1}{B}(m_c - m_t), \\
\frac{dC}{dt} &= \frac{1}{\tau}(C_{ss} - C),
\end{aligned}$$

where m_c (resp. m_t) denotes the nondimensional compressor (resp. throttle) mass flow rate, Δ_p (resp. C) denotes the nondimensional plenum (resp. compressor) pressure rise, and C_{ss} and F denote the nondimensional *static* compressor pressure rise and throttle pressure drop, respectively. The parameter B is proportional to the square root of the ratio of plenum/compressor volume for a constant rotor speed; the definitions of the three parameters, B, G, and τ in terms of physical system parameters are given in [1]. The throttle characteristic F is given by the orifice equation

$$F = \left(\frac{A_c^2}{A_t^2}\right) m_t^2$$

where A_c/A_t is the compressor/throttle cross section ratio. The steady state compressor characteristic C_{ss} used in this work approximates Greitzer's experimentally determined characteristic with cubic splines (see Fig. 1).

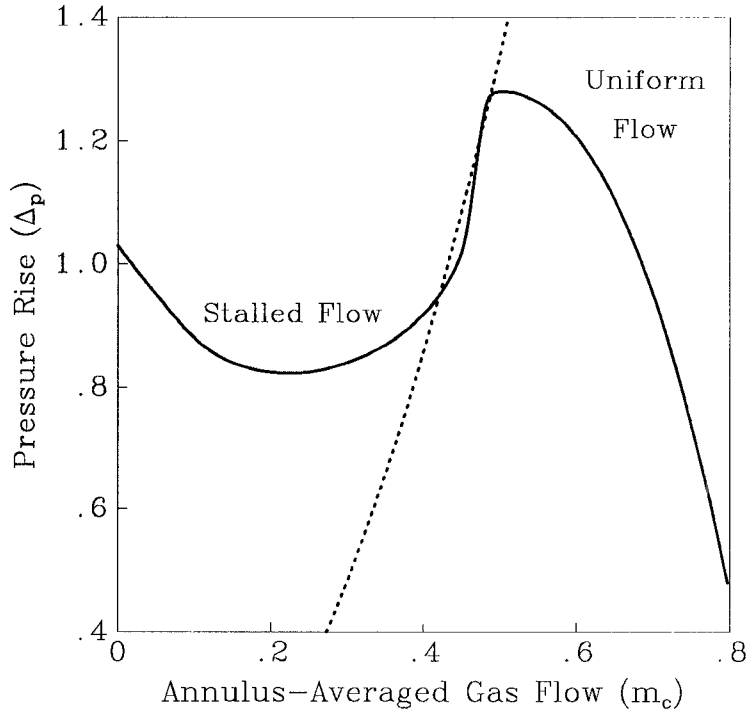

Figure 1 The compressor characteristic (solid curve) used in this study (c.f. [7]) and the throttle characteristic for $\gamma = 0.432$ (dashed curve).

Since the relaxation time τ is small relative to the surge cycle frequency and other important dynamical features, it has been shown [8] that the full, fourth-order system can be reduced to the second-order model:

$$\frac{dm_c}{dt} = B(C_{ss} - \Delta_p),$$
$$\frac{d\Delta_p}{dt} = \frac{1}{B}(m_c - \gamma\sqrt{\Delta_p}),$$

where

$$\gamma = \frac{A_t}{A_c}.$$

An important aspect of this simplification is that only two parameter remain, the B parameter and the throttle opening γ, and so a complete bifurcation analysis is more easily done in the two-parameter plane for a particular compressor characteristic. Comparisons with the full, fourth-order system can be found in [9].

Computing Equilibrium Solutions

At steady-flow equilibrium, the pressure rise through the compressor

$$\Delta_p = C_{ss}(m_c)$$

equals the pressure drop through the throttle (or system resistance)

$$\Delta_p = \left(\frac{m_c}{\gamma}\right)^2$$

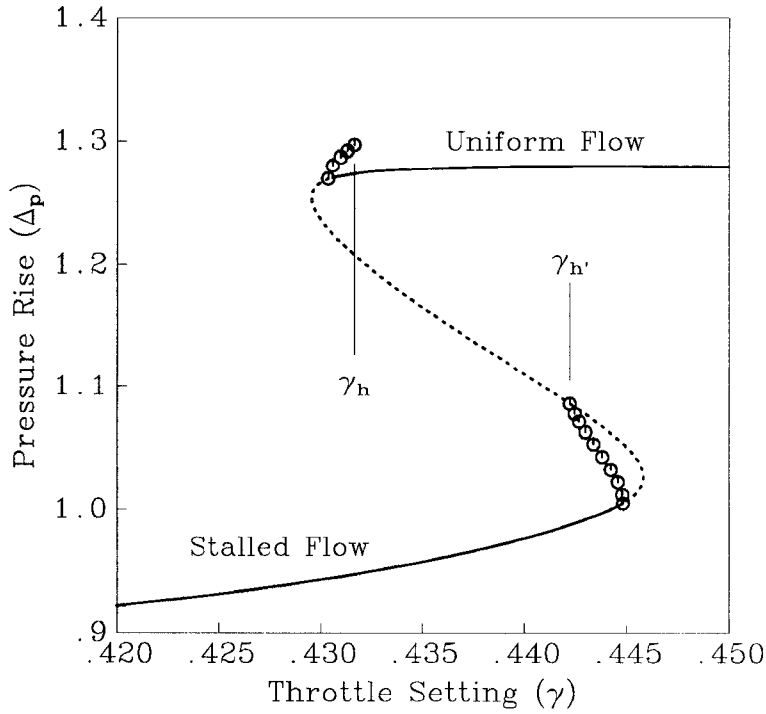

Figure 2 A bifurcation diagram illustrating how equilibrium solutions change as a function of throttle opening for a fixed value of $B = 0.27$. Solid curves represent stable steady-flow solutions, the dashed section indicates an unstable solution branch, and the open circles denote the maximum amplitude of unstable surge oscillations.

and the gas flux through the compressor also equals the flow through the throttle. Steady-flow equilibrium solutions can be graphically represented in phase space by the intersections of the compressor and throttle characteristics (see Fig. 1). Thus, when the throttle is opened wide (large γ), the throttle characteristic intersects the compressor characteristic in its higher-m_c section and gives a unique uniform-flow solution. As the throttle is closed (γ is reduced), the characteristics intersect at three points giving a high-Δ_p uniform-flow solution, a low-Δ_p stalled-flow solution, and a mid-range-Δ_p stalled-flow solution that will be shown to have saddle-type stability and so plays a crucial role in the over-all dynamical behavior. As γ is decreased further, the characteristics once again intersect at a single point, but now giving a unique low-Δ_p stalled-flow solution.

This means the steady-flow solution branch in the phase space (Fig. 1) is parameterized by the throttle opening γ. Thus, an equivalent way of representing equilibrium solutions is to plot the values of one of the states versus the throttle opening parameter. These *bifurcation diagrams* also can contain periodic (surging flow) solution branches by plotting the peak amplitude of the limit cycles as a function of γ. The advantages bifurcation diagrams have over diagrams such as Fig. 1 are that we can immediately determine the number of equilibria that exist for a particular throttle opening and it is easier to understand the transitions which take place as the throttle is *slowly* opened or closed.

This diagram can be interpreted by considering the system with the throttle opened wide (large γ). We see that the uniform-flow solution is stable and appears to the the unique solution in this range of γ. As γ is decreased below $\gamma = 0.4448$, the uniform-flow solution remains locally stable, but coexists with a locally stable stalled-flow solution. This means that perturbations of

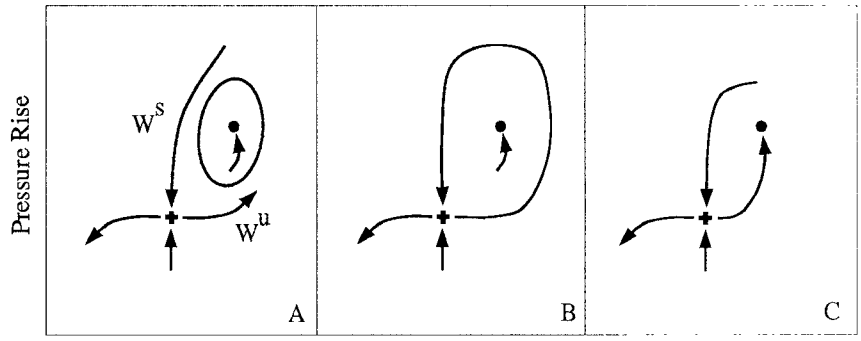

Figure 3 A sequence of phase portraits illustrating a global (homoclinic) bifurcation. Phase portrait A corresponds to $\gamma < \gamma_h$, B to $\gamma = \gamma_h$, and C to $\gamma > \gamma_h$.

finite size will destabilize the uniform-flow operating point. At $\gamma = 0.4306$, the uniform-flow operating point becomes unstable when the eigenvalues of its linearization cross the imaginary axis as a complex-conjugate pair. This is an example of a subcritical Hopf bifurcation since the periodic solution (a surge frequency oscillation) born at the bifurcation point is unstable. This means that slowly closing the throttle through the instability point will give a time trace showing the system settling down to the steady stalled-flow equilibrium after the instability margin (the Hopf bifurcation point) is crossed. While the post instability behavior is simple to predict at this value of B, in general, the more detailed analysis which follows is required. Another important point is that the Hopf bifurcation precedes (with respect to closing the throttle) the saddle-node bifurcation marking the stall point in this model. This is also not necessarily the general case.

Homoclinic Connections

The bifurcation diagram (Fig. 2) contains a plot of equilibrium solutions found for a particular value of B ($B = 0.27$) as a function of γ. We see that the periodic solutions abruptly end at $\gamma = \gamma_h = 0.4316$ and the other at $\gamma = \gamma_{h'} = 0.4422$. This is due to the destruction of the limit cycles during homoclinic bifurcations.

The sequence of phase portraits shown in Fig. 3 illustrates the mechanism responsible for the destruction of limit cycles in the case of those born at the Hopf bifurcation point of the uniform-flow solution branch. For $\gamma < \gamma_h$, a saddle point coexists with a stable fixed point inside an unstable limit cycle in the region of phase space relevant to this bifurcation. The limit cycle grows in amplitude with increasing γ, and finally runs into the saddle at $\gamma = \gamma_h$. This nontransversal crossing of the saddle stable and unstable manifolds[1] results in a limit cycle of infinite period. After the bifurcation point ($\gamma > \gamma_h$), the unstable limit cycle no longer exists and so the basin of attraction boundary of the upper stable fixed point now consists of the saddle-stable manifold.

The parameter values at which the homoclinic connections take place can be computed with a shooting algorithm. This is particularly easy to implement in the 2nd-order model since the stable and unstable manifolds are one-dimensional. The numerical algorithm consists of the

[1] Roughly speaking, the saddle stable manifold (W^s) consists of all initial conditions in phase space which asymptotically approach the saddle point in forward time; the saddle unstable manifold (W^u) consists of all points which asymptotically approach the saddle in reverse time. More precise definitions can be found in [10].

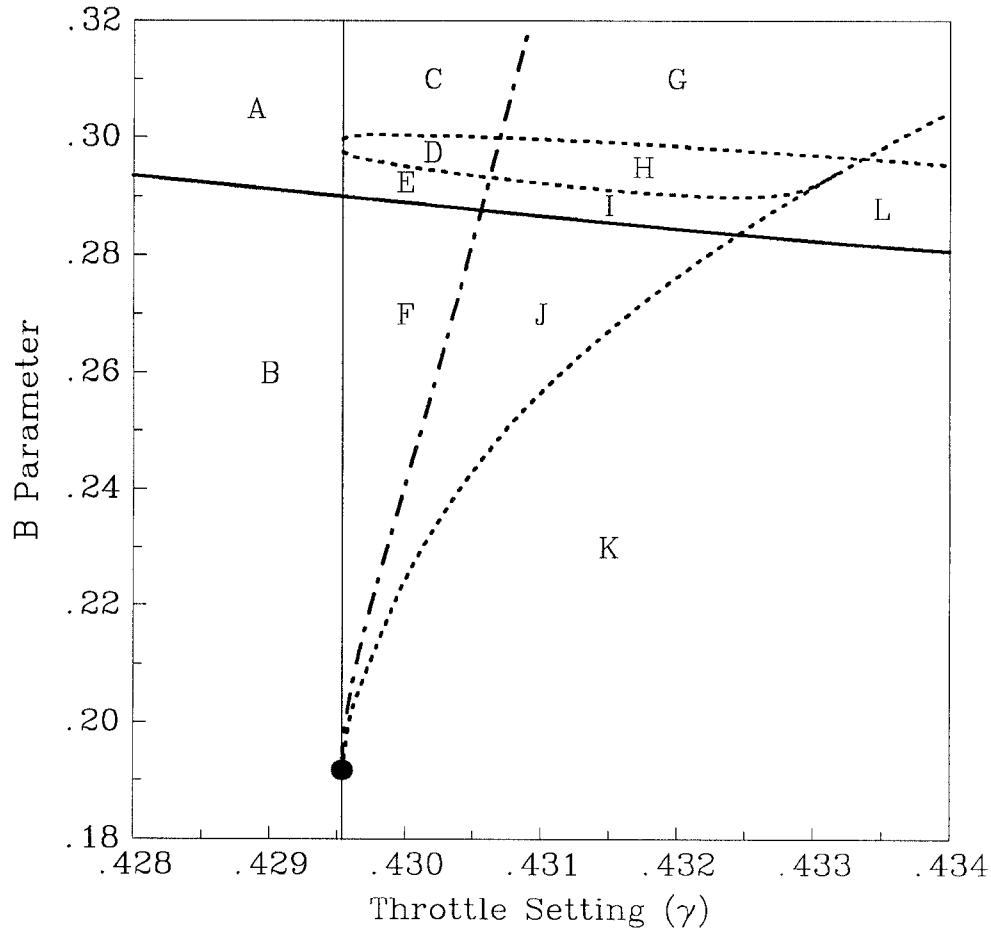

Figure 4 A two-parameter bifurcation diagram illustrating the parameter regions of qualitatively-different phase portraits. The thin, solid line represents a fixed-point saddle-node bifurcation, the thicker solid curve corresponds to a saddle-node of limit cycles, the fixed-point Hopf bifurcation is maked by a dash-dot curve, and the saddle (homoclinic) connections by the dotted curves.

following three steps: 1) a local approximation of the saddle-stable manifold (W^s_{loc}) is made (the zeroth-order approximation is the line passing through the saddle parallel to the saddle-stable eigenvector E^s); 2) an initial condition is chosen on W^s_{loc} and integrated backward in time until the trajectory intersects a test line parallel to E^s; 3) the distance from this intersection point and the test point (defined by the intersection of the test line and saddle-unstable eigenvector E^u) is used as a function $\mathcal{D}(\gamma, B)$ in a Newton-Raphson iteration to determine $\mathcal{D} = 0$. This iterative scheme will converge on the global bifurcation when a sufficiently accurate initial guess for the parameters is given.

Determining B_c

The saddle-node bifurcations marking the boundaries of the hysteresis loop of stalled/uniform-flow solutions is determined solely by the intersections of the throttle and compressor characteristics. This means their locations (γ values) will not change as a function of B. However, the locations of the Hopf bifurcation points, the saddle-node bifurcations of limit cycles, and the homoclinic bifurcations will vary with B, and so it is useful to plot the locations

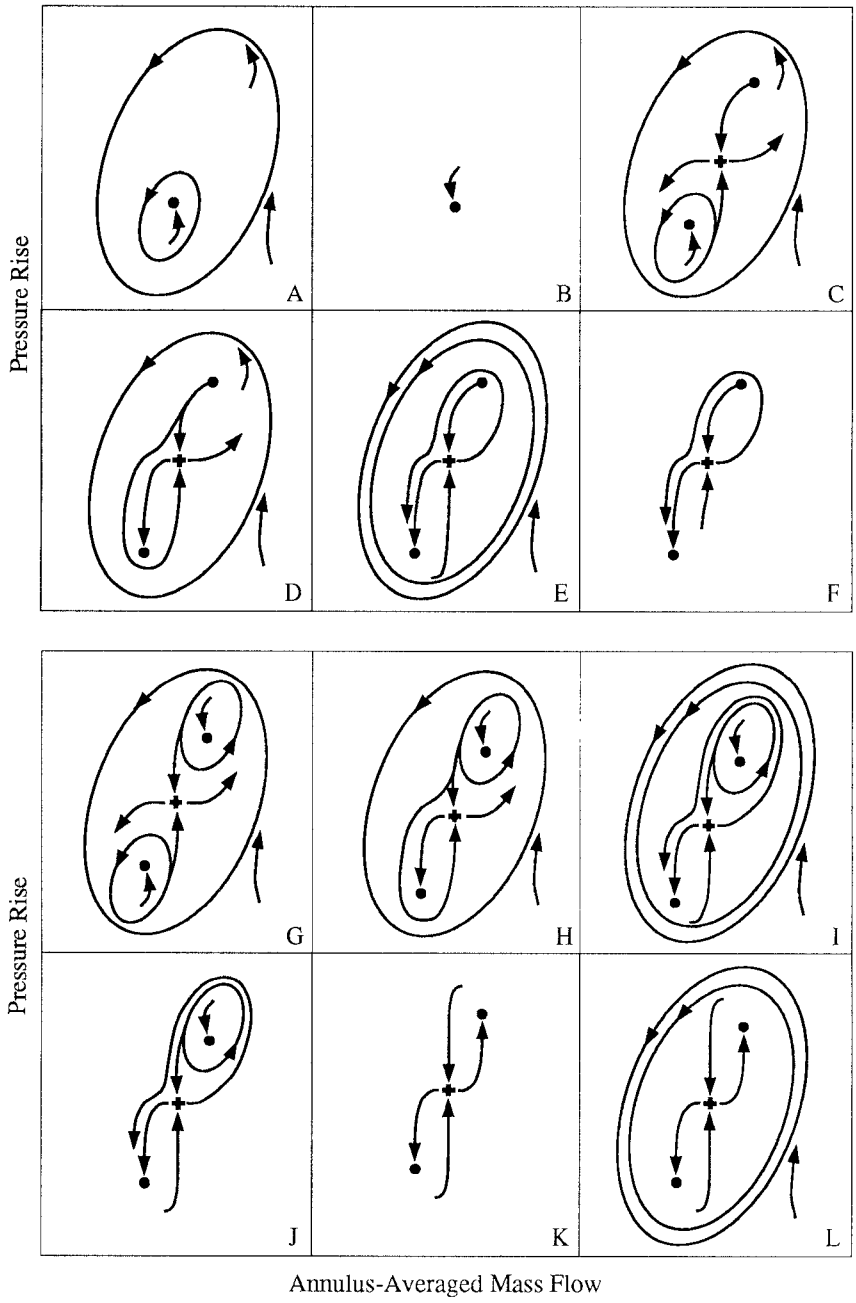

Figure 5 The phase portraits corresponding to regions of qualitatively-different dynamical behavior. Stable and unstable fixed points are represented by • and saddle-type fixed points by +.

of these bifurcations in the (γ, B)-plane. Computation of the saddle-node and Hopf bifurcation loci can be done without modification to continuation software packages such as AUTO. Continuation of the homoclinic connections required using the shooting algorithm in conjunction with the continuation package. Constructing this type of bifurcation diagram (Fig. 4) gives a complete picture of the qualitatively-different dynamical behaviors in the parameter space (throttle position and B, for a particular compressor characteristic).

Having constructed the two-parameter bifurcation diagram, we can determine the post-instability behavior from the phase portraits corresponding to parameter regions adjacent to

the curve in this plane which separates parameter values where the uniform-flow solution is locally stable from regions where it is unstable. For $B \in (0.0.1917]$, this is the saddle-node bifurcation which destroys the uniform-flow solution. For $B \geq 0.1917$, the Hopf bifurcation locus is the boundary marking the destabilization of the uniform-flow solution. Having defined the (local) instability margin in the parameter plane (Fig. 4), we now consider the qualitatively different pre- and post-instability behaviors bordering this curve (Fig. 5).

The K $\rightarrow$ B transition: For small values of B and in the throttle opening range where the stable uniform-flow solution coexists with a stable rotating stall equilibrium, we find phase portraits qualitatively similar to the one shown in Fig. 5K. In this phase portrait, the uniform-flow solution is the point in the upper right-hand side of the diagram, and the initial conditions in the phase space which asymptotically approach it are separated from those which asymptotically approach the rotating stall equilibrium (the fixed point in the lower left corner) by the stable manifold of the saddle point. When the throttle is slowly closed and B is held constant, the saddle point and the uniform-flow solution come together and are annihilated during the saddle-node bifurcation, leaving the rotating stall as the only equilibrium (phase portrait B). This means the post instability behavior is guaranteed to be rotating stall for small values of B; a time trace corresponding to slowly closing the throttle through the boundary separating regions K and B is shown in Fig. 6a.

The J $\rightarrow$ F transition: Above the double-zero eigenvalue point[2] ($B = 0.1917, \gamma = 0.4295$), the uniform-flow operating point is destabilized during throttle closing by an unstable limit cycle (of surge frequency) collapsing onto the operating point during a Hopf bifurcation. The sequence of bifurcations relevant to this transition starts with phase portrait J, which is similar to K discussed above except that the boundary separating the two basins of attraction consists of the unstable limit cycle. When the throttle is closed and the uniform-flow solution becomes unstable, we see that the fixed points remain and all initial conditions (except for the saddle-stable manifold and the fixed points themselves) asymptotically approach the rotating stall equilibrium (Fig. 5F).

The I $\rightarrow$ E transition: Parameter region I lies above the saddle-node bifurcation of limit cycles curve, and so three attractors (the large amplitude surge oscillation, and the rotating stall and uniform-flow equilibria) coexist in this region of parameter values. The existence of the surge cycle does not necessarily mean that the post instability behavior will be surge—in fact, if the throttle is closed slowly and only to a point within region E, the compressor will *stall*. The unstable surge cycle acts as a basin of attraction boundary of the stable surge cycle, and so surge can only occur is there is a sufficiently large perturbation in the phase space or if the throttle is closed quickly and so far as to enter region A.

The H $\rightarrow$ D transition: As B is increased from a point in region I into H (or from region E into D), the large amplitude unstable surge cycle shrinks until it is destroyed during a homoclinic bifurcation. This means both sides of the saddle-stable manifold must approach the same unstable equilibrium *in reverse time* in regions H and D. The importance of this is made clear by considering a phase portrait corresponding to parameter values near the lower-B boundary of region D. For these parameter values, the segment of W^s which approaches the saddle from its lower side appears to "peel" away from the right-hand side of the W^s segment

[2] This is where a Hopf bifurcation locus ends at a fixed-point saddle-node bifurcation curve, and so the bifurcating fixed point has two pure-real zero eigenvalues at this set of parameter values. It has been shown that a locus of homoclinic bifurcations must also emanate from this point [10].

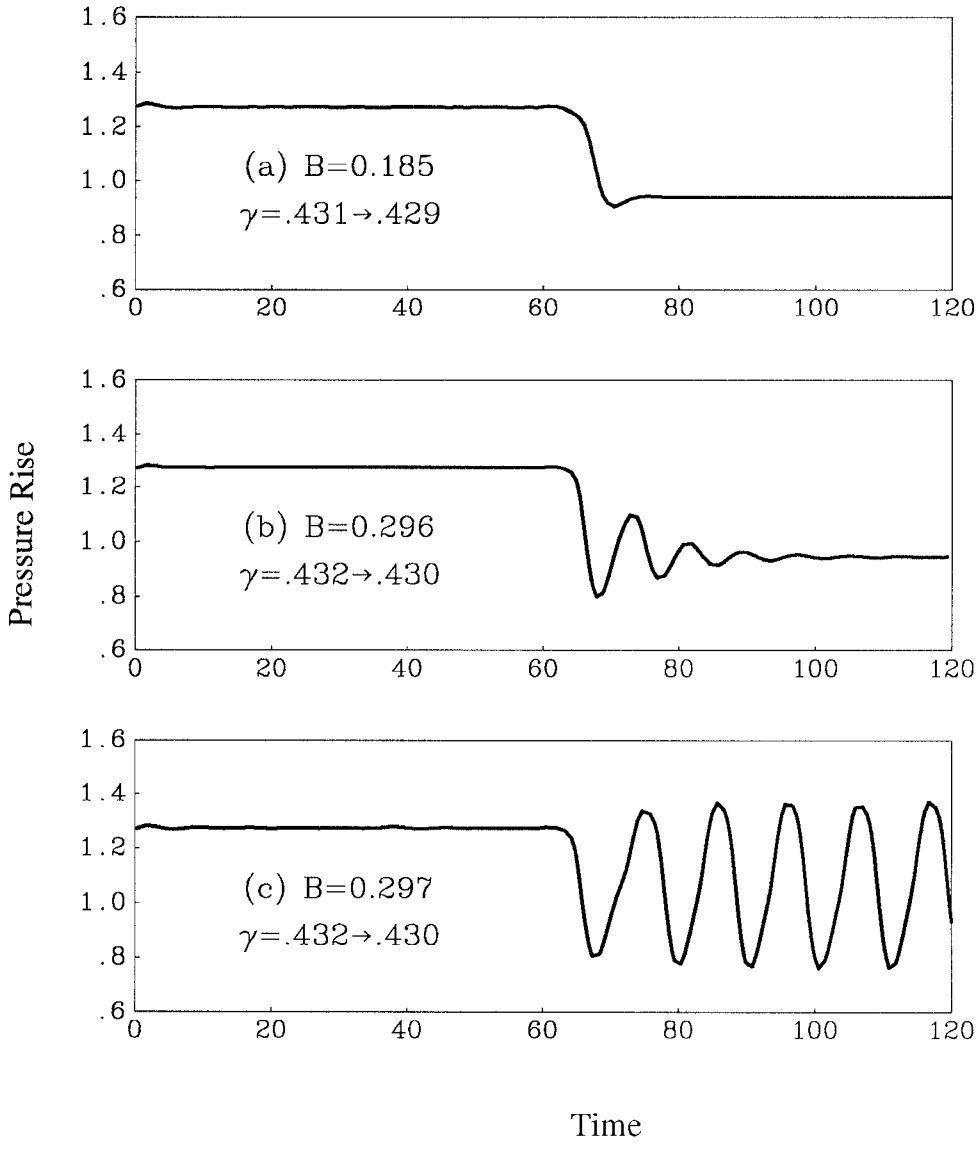

Figure 6 Time traces illustrating the dynamical behavior exhibited for different values of B. The uppermost (a) corresponds to a transition from region K to region B (of Fig. 4), and (b) and (c) show how the post-instability behavior varies with B in the transition from region H to D. The value of γ is switched from the higher value shown to the lower at $t = 60$.

approaching the saddle from the top (see Fig. 7a). This means that initial conditions in the neighborhood of the unstable uniform-flow point will be more likely to asymptotically approach the rotating stall equilibrium for lower-B values in region D, although there is a finite possibility of surge. This possibility increases to the point of certainty as B is increased within region D, since the W^s segment that approaches the saddle from below rotates around the uniform flow equilibrium in a counter-clockwise manner (see Fig. 7b) giving an increasing percentage of the phase space surrounding the unstable uniform-flow point in the basin of attraction of the surge cycle. The net effect of these changes can be seen in time traces (b) and (c) of Fig. 6, where closing the throttle in the low-B range of the H to D transition is more likely to result in stall (Fig. 6b) and more likely to give surge (Fig. 6c) in the high-B range.

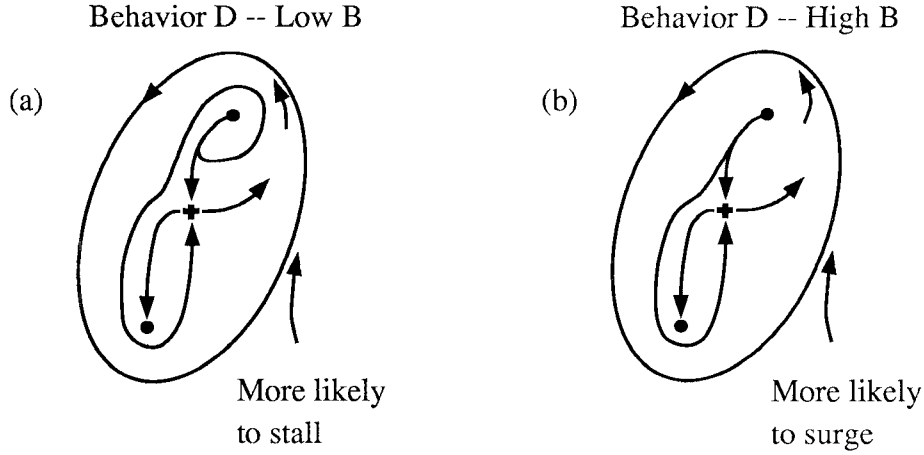

Figure 7 The different "types" of phase portraits corresponding to behavior D.

The G $\rightarrow$ C transition: In the B-range of behaviors G and C, a small amplitude unstable oscillation (a modulated traveling wave in terms of the true distributed parameter system) defines the basin of attraction of the rotating stall equilibrium. This limit cycle persists during the G to C transition, and so all initial conditions in the neighborhood of the unstable uniform-flow solution asymptotically approach the large amplitude surge oscillation (phase portrait C). While there are additional bifurcations that take place at higher values of B than represented in Fig. 4, none appear to affect the post-instability behavior of surge for $B > 0.32$.

Multistability

To this point, we have only considered the problem of determining the long-term compression system behavior when the *locally* stable uniform-flow operating point becomes *locally* unstable. It has been observed that perturbations of sufficient magnitude will destabilize a uniform-flow operating point otherwise stable to infinitesimal disturbances [11]. This signals the coexistence of attracting equilibria—multistability. We can use the same numerical analysis techniques described in the previous sections to determine the (throttle opening, B)-parameter ranges where multistability exists and then to *quantify* the destabilizing disturbances.

We first consider the problem of determining the parameter region of multistability. This parameter range consists of the intersection of the region where the uniform-flow solution is locally stable with the union of the ranges where the other attractors (stable rotating stall equilibria and stable surge cycles) exist. In general, it is difficult to prove that all of the attractors for a particular nonlinear system have been found, but careful analysis plus a consistent picture of the bifurcation scenarios assures that most, if not all, regions of multistability have been found.

Computing the parameter region where the uniform-flow solution is locally stable was discussed in the previous section. It consists of all the values of γ to the right of the saddle-node bifurcation of the uniform-flow/saddle points (at $\gamma = 0.4295$) when $B \leq B_{00L}$, where B_{00L} is one of the double-zero eigenvalue points shown in Fig. 8. For $B \geq B_{00L}$, the boundary consists of the fixed-point Hopf curve, and the region of local stability is all γ values to the right of this curve.

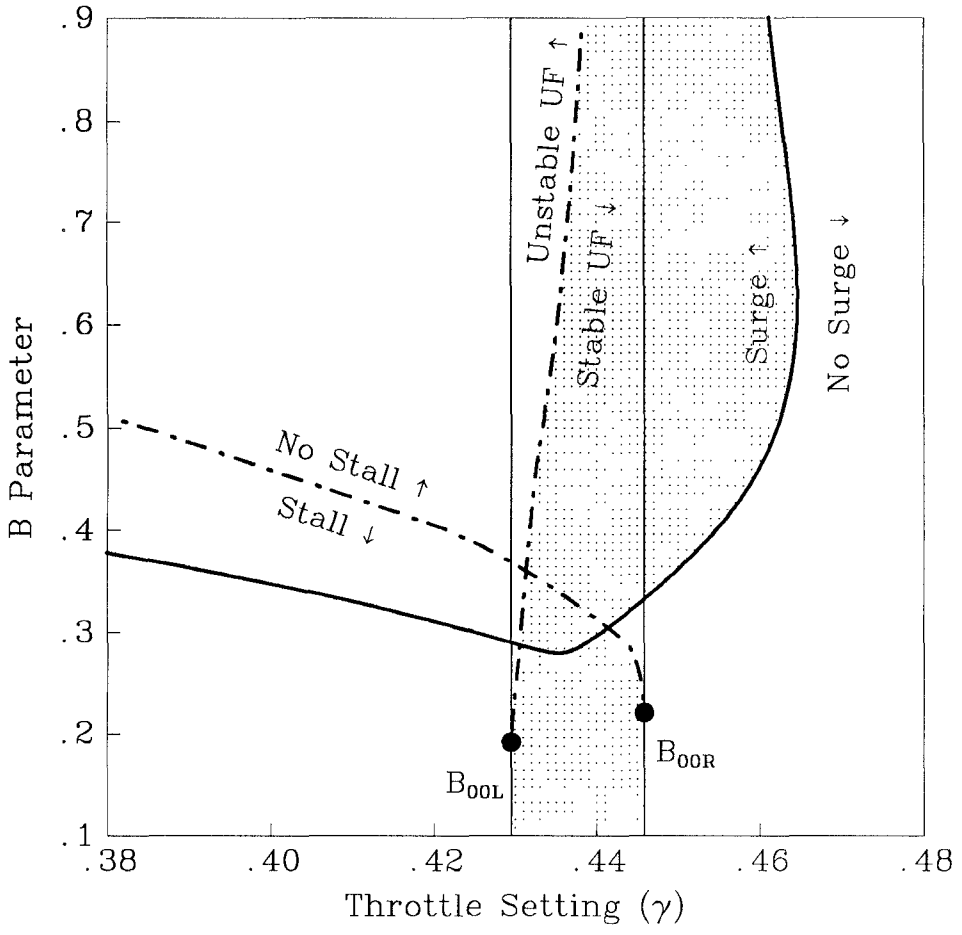

Figure 8 A two-parameter bifurcation diagram illustrating the region of multistability (the shaded area) and the different bifurcations which determine the boundaries of this region.

The region where the locally-stable rotating stall equilibria exist is found in an analogous manner: a stable rotating stall fixed point is found for all γ values to the *left* of the saddle-node bifurcation of the stalled-flow/saddle points (at $\gamma = 0.4458$) when $B \leq B_{00R}$. For $B \geq B_{00R}$, the boundary consists of the stalled-flow Hopf curve, and the region of local stability is all γ values to the left of and below this curve.

In the parameter range studied for this particular compression system, we find no degenerate Hopf bifurcation points and we can prove that no stable limit cycles (pure surge or modulated traveling waves born off the stalled-flow solution locus) are born/destroyed via homoclinic connections[3]. This means stable oscillatory solutions will lie entirely inside the boundaries defined by limit cycle saddle-node bifurcations.

Since the multistability boundaries consist solely of "conventional" bifurcations (saddle-node bifurcations of fixed points and periodic solutions, and Hopf bifurcations of fixed points), they can be computed with standard numerical bifurcation analysis packages such as AUTO.

[3] It is easy to show that the trace of the linearization of the saddle points in the neighborhood of the saddle-node bifurcations is positive for all B above the double-zero eigenvalue points. It then follows from Theorem 6.1.1 of [10] that only unstable limit cycles can be involved in homoclinic bifurcations under these conditions.

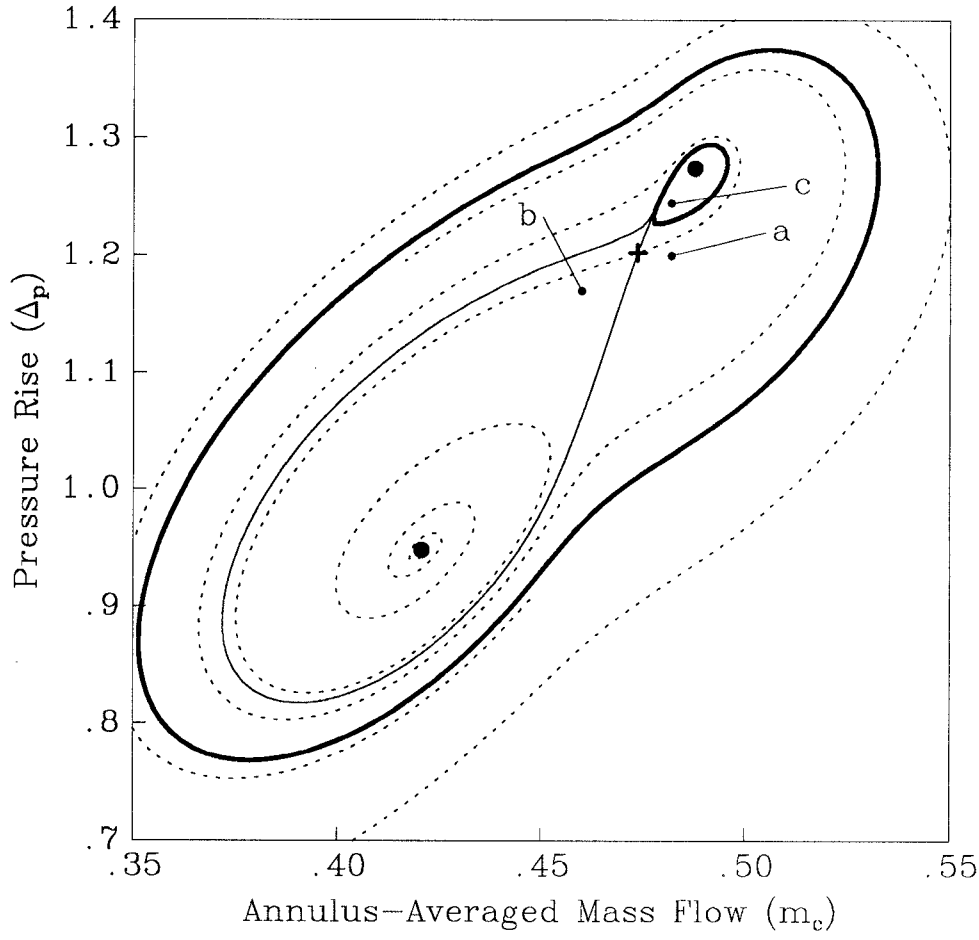

Figure 9 A phase portrait with parameter values ($B = 0.295, \gamma = 0.432$) taken from region H. The thicker closed curves denote limit cycle solutions.

The final results are illustrated in Fig. 8, with the shaded region showing the relatively large range of multistability.

Basins of Attraction

Having computed the parameter region of multistability, we can compute the actual phase portraits (as opposed to the hand-drawn versions in Figs. 3, 5, and 7). For example, in Fig. 9, a computed phase portrait is shown corresponding to behavior H where the stable uniform operating point coexists with a stable rotating stall equilibrium and a stable surge cycle. In the following figures, we show time traces corresponding to different types of perturbations (in magnitude and direction) resulting in the system ultimately settling down to the two different undesirable attractors. The basin boundaries separating sets of initial conditions leading to the different attractors can be computed accurately with established numerical [12] and computational techniques [13].

To illustrate the effects of multistability and how destabilizing perturbations are quantified, consider the fate of the set of initial conditions marked by point (c) in Fig. 9. Since this point

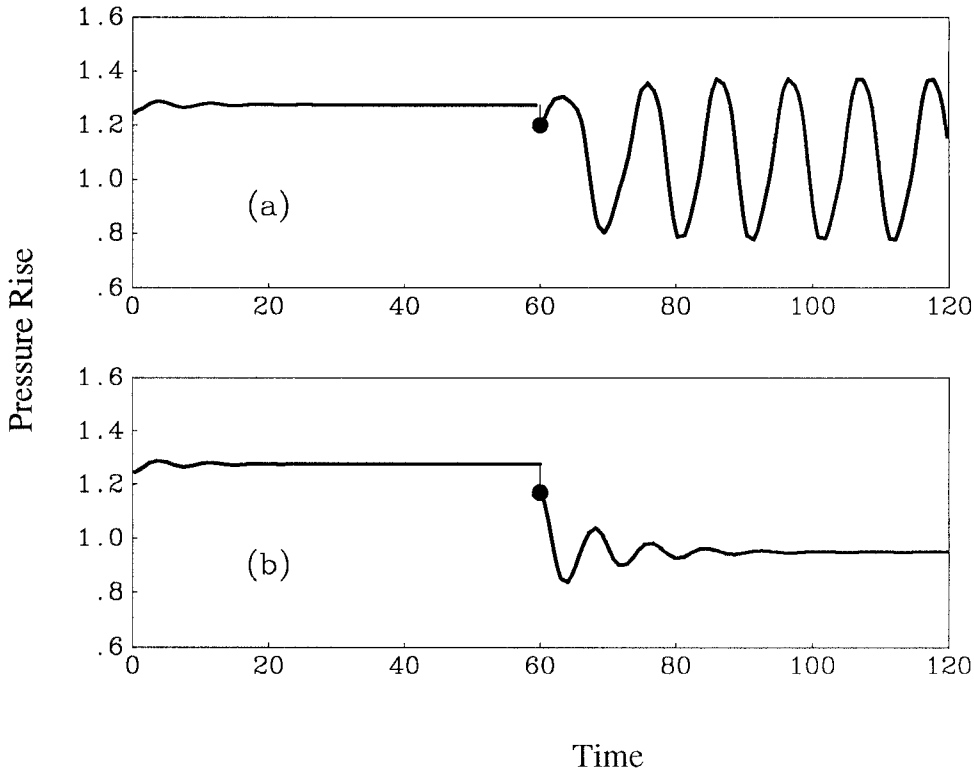

Figure 10 Time traces showing the compression system asymptotically approaching the stable uniform-flow fixed point during the first 60 time units of operation and the post-perturbation behavior when the perturbation (points a and b of Fig. 9) lies in the basin of attraction of the surge cycle (a), and rotating stall equilibrium (b).

lies inside the unstable limit cycle defining the basin of attraction boundary of the uniform-flow solution, the system will asymptotically approach this fixed point (see the initial 60 time units of each time trace presented in Fig. 10). If, after the system is allowed to approach the uniform-flow solution, the states are perturbed so that immediately after the perturbation the instantaneous flow and plenum pressure rise values are those marked by point (a) in Fig. 9, the compressor will ultimately surge (see the second half of time trace (a) of Fig. 10) rather than return to the uniform-flow operating point since point (a) lies inside the surge cycle basin of attraction. Similarly, if the system is perturbed so that (m_c, Δ_p) corresponds to point (b) of Fig. 9, the compressor will stall (see Fig. 10b) rather than return to the uniform-flow operating point since point (b) lies in the basin of attraction of the rotating stall equilibrium. The rotating stall basin of attraction boundary consists of the saddle-stable manifold, shown as the thinner solid curves of Fig. 9. The thin dotted trajectories originating at the saddle point (marked by a $+$) are a portion of the saddle-unstable manifold.

Conclusions

We have used global bifurcation analysis to establish the mechanisms responsible for the transition from stall to surge as the post-instability behavior as a function of the B parameter. Using an approximation of the experimentally determined characteristic of Greitzer [7] and a low-order compression system model, we find the critical value of B to be in the range of

(0.2932,0.3000). A precise value of B_c cannot be given by the nature of the changes in the phase space structures which organize the dynamics over this range of B.

In addition to predicting the long-term system dynamics after the desired operating point becomes locally unstable, the methods of analysis used also uncover parameter ranges where the locally stable uniform-flow operating point coexists with a stable surge cycle and/or a rotating stall equilibrium. The computational techniques presented were shown to be useful for quantifying destabilizing perturbations in multistable situations.

An advantage of using a low-order compression system model is that a detailed bifurcation analysis was possible. This gave a clear, *complete* picture of the dynamical behavior of this system. This provides a starting point for analysis of more detailed models which can account for the spatial nature of rotating stall. The analysis presented in this work provides a basis from which to begin a rigorous bifurcation analysis of the post-instability behavior of the true, distributed-parameter compression systems.

Acknowledgments

This work was supported in part by the General Electric Company, by NSF Grants ECS-86-57561 and CDR-88-03012, and by the AFOSR University Research Initiative Program under Grant AFOSR-90-0015. RAA was supported by the Systems Research Center under NSF Grant ECD-88-03012-06.

References

[1] Greitzer, E. M. (1976). Surge and rotating stall in axial flow compressor, Part I: Theoretical compression system model. *ASME J. Engineering for Power*, **98**, 190-198.

[2] McCaughan, F. E. (1989). Application of bifurcation theory to axial flow compressor instability. *ASME J. Turbomachinery*, **111**, 426-433.

[3] Doedel, E. J. (1981). AUTO: A program for the automatic bifurcation analysis of autonomous systems. *Cong. Num.*, **30**, 265-284.

[4] Moore, F. K. and E. M. Greitzer (1986). A theory of post-stall transients in axial compression systems: Part I–Development of equations. *ASME J. Engineering for Gas Turbines and Power*, **108**, 68-76.

[5] Lavrich P. L. (1988). Time resolved measurements of rotating stall in axial flow compressors. *MIT GTL Report 194.*

[6] Adomaitis, R. A. and E. H. Abed (1992). The dynamics and control of axial-flow gas compressors. *SIAM Conf. on Control and Appl.*, Minneapolis.

[7] Greitzer, E. M. (1976). Surge and rotating stall in axial flow compressor, Part II: Experimental results and comparison with theory. *ASME J. Engineering for Power*, **98**, 199-217.

[8] Abed E. H., P. K. Houpt, and W. M. Hosny (1990). Bifurcation analysis of surge and rotating stall in axial flow compressors. *Proc. 1990 American Control Conference*, 2239-2246.

[9] Liaw, D. -C., R. A. Adomaitis, and E. H. Abed (1991). Nonlinear dynamics of axial flow compressors: A parametric study. *SRC Technical Report TR 91-32.*

[10] Guckenheimer, J. and P. Holmes (1983). *Nonlinear Oscillations, Dynamical Systems, and Bifurcations of Vector Fields*. Springer-Verlag, New York.

[11] Day, I. J. (1991). Stall inception in axial flow compressors. *Proc. 1991 ASME Gas Turbine Conf.*, Orlando.

[12] Franceschini, V. and L. Russo (1981). Stable and unstable manifolds of the Henon mapping. *J. Stat. Phys.*, **25**, 757-769.

[13] You, Z., E. J. Kostelich, and J. A. Yorke (1991). Calculating stable and unstable manifolds. *Int'l J. Bifurcation and Chaos*, **1**, 605-623.